



Constitutive modeling of ultra-fine-grained titanium flow stress for machining temperature prediction

Jinqiang Ning¹ · Vinh Nguyen¹ · Yong Huang² · Karl T. Hartwig³ · Steven Y. Liang¹

Received: 15 May 2019 / Accepted: 22 July 2019 / Published online: 1 August 2019
© Zhejiang University Press 2019

Abstract

This work investigates the machining temperatures of ultra-fine-grained titanium (UFG Ti), prepared by equal channel angular extrusion, through analytical modeling. UFG Ti has great usefulness in biomedical applications because of its high mechanical strength, sufficient manufacturability, and high biocompatibility. The temperatures were predicted using a physics-based predictive model based on material constitutive relation and mechanics of the orthogonal cutting process. The minimization between the stress calculated using Johnson–Cook constitutive model and the same stress calculated using mechanics model yields the estimation of machining temperatures at two deformation zones. Good agreements are observed upon validation to the values reported in the literature. The machinability of UFG Ti is investigated by comparing its machining temperature to that of Ti–6Al–4V alloy under the same cutting conditions. Significantly lower temperatures are observed in machining UFG Ti. The computational efficiency of the presented model is investigated by comparing its average computational time (~0.5 s) to that of a widely used modified chip formation model (8900 s) with comparable prediction accuracy. This work extends the applicability of the presented temperature model to a broader class of materials, specifically ultra-fine-grained metals. The high computational efficiency allows the *in situ* temperature prediction and optimization of temperature condition with process parameters planning.

Keywords Ultra-fine-grained titanium · Analytical modeling · High computational efficiency · Johnson–Cook model · Cutting mechanics

Introduction

Ultra-fine-grained titanium (UFG Ti) has great potential to replace the widely used Ti–6Al–4V alloy in biomedical applications because of its high mechanical strength, sufficient manufacturability, and high biocompatibility with human cells and tissues. It has a comparable yield strength to that of Ti–6Al–4V [1]. The machinability of UFG Ti was

investigated in machining forces [2]. The cutting forces of UFG Ti are significantly lower than that of Ti–6Al–4V under the same cutting conditions. The biocompatibility of UFG Ti was investigated with cell adhesion and proliferation, from which the UFG Ti was reported with higher biocompatibility than Ti–6Al–4V because aluminum and vanadium elements are toxic to human cells and tissues [3]. A severe plastic deformation (SPD) process, namely equal channel angular extrusion (ECAE), was commonly employed in preparing UFG Ti, in which the bulk materials go through a rigid die with the large-angle channel in multiple passes. More details about ECAE process can be found in the references [4–7], in which the influence of process details including process route, scale, and rolling, extrusion on the microstructure, and mechanical properties was investigated.

Machining is needed to transform the bulk material into a finished product, which is widely used because of its fast speed and applicability to a broad class of materials. It is well known that elevated temperature has a negative

✉ Jinqiang Ning
jinqiangning@gatech.edu

¹ George W. Woodruff School of Mechanical Engineering, Georgia Institute of Technology, 801 Ferst Drive, Atlanta, GA 30332, USA

² Department of Mechanical and Aerospace Engineering, University of Florida, 231 MAE-A, P. O. Box 116250, Gainesville, FL 32611, USA

³ Department of Mechanical Engineering, Texas A&M University, 3123 TAMU, College Station, TX 77843-3123, USA

influence on tool performance and quality of the machined part because it softens tool materials and increases diffusion.

Temperature measurement through experiment is difficult and inconvenient due to the complex contact phenomena at the chip formation zone and restricted accessibility during the machining process [8, 9]. Numerical models were developed based on finite element analysis (FEA) to predict the machining force, temperature, residual stress, and chip morphology [10–14]. Although the developed numerical models have made considerable progress in the prediction of the machining process, the expensive computational cost is still the major drawback.

Analytical models were developed based on physics to predict the machining forces, temperature, and residual stress [15–21]. Analytical model has promising high computational efficiency without resorting to FEA or any iteration-based simulations. A chip formation model, as originally proposed by Oxley, was used to predict machining forces in orthogonal cutting, in which the uniform machining temperatures at two deformation zones were calculated as intermediate variables [22]. Another temperature model considering heat sources at two deformation zones, as originally proposed by Komanduri et al. [23], was often used with the chip formation model to predict temperature distribution at chip formation zone. However, the temperature-dependent material properties of the workpiece including thermal conductivity and specific heat are needed but must be obtained from extensive material property tests. In addition, the exhaustive search method and complex calculations in the chip formation model decrease computational efficiency.

In this work, the machining temperatures in orthogonal cutting of UFG Ti were investigated through analytical modeling. The UFG Ti workpiece was prepared by an ECAE process and then tested in the orthogonal cutting under various cutting conditions. The details of the ECAE process can be found in the previous work [24]. The machining temperatures at two deformation zones, namely primary shear zone (PSZ) and second shear zone (SSZ), were predicted using an analytical model developed based on material constitutive relation and mechanics of the orthogonal cutting process. The predicted temperatures are validated to the values reported in the literature [2]. The computational efficiency of the employed analytical model was investigated with a comparison of computational time to the widely used modified chip formation model. In addition, the machinability of UFG Ti was investigated by comparing the machining temperatures to that of Ti-6Al-4V, which is widely used in lightweight engineering applications and biomedical applications.

Methodology

The machining temperatures are predicted by the analytical model based on material constitutive relation and mechanics of the orthogonal cutting process. Johnson–Cook constitutive model (J–C model) is chosen in temperature prediction because it is effective, simple, and easy to use. The average temperatures at PSZ (T_{AB}) and SSZ (T_{int}) are determined by minimizing the difference between the calculated shear stress using J–C model and the calculated shear stress using mechanics model at PSZ and SSZ, respectively. The reliable and easily measurable cutting force and chip thickness were used as inputs, which can be experimentally measured by a piezoelectric dynamometer and micrometer, respectively [25]. The two strain rate constants (C_0 in a range of 2 and 10 with 0.1 increment and δ in a range between 0.005 and 0.2 with 0.005 increment are determined from minimization of the difference between calculated stresses.

The flow stress can be calculated using the J–C model with considerations of strain hardening effect, strain rate hardening effect, and thermal soften effect. It can be expressed as

$$\sigma = (A + B\epsilon^n) \left(1 + C \ln \left(\frac{\dot{\epsilon}}{\dot{\epsilon}_0} \right) \right) \left(1 - \left(\frac{T - T_0}{T_m - T_0} \right)^m \right) \quad (1)$$

where A , B , C , m , n are five materials parameters (J–C constants), which can be determined using various methods such as split Hopkinson pressure bar (SHPB) tests, numerical methods, or analytical methods [26–30]. ϵ , $\dot{\epsilon}$, T denote strain, strain rate, and temperature, respectively.

The flow stress can also be calculated using the mechanics model in orthogonal cutting configuration. The orthogonal cutting can be performed by turning a tubular workpiece as illustrated in Fig. 1. The chip formation zone in orthogonal cutting is illustrated in Fig. 2, where α is the rake angle, ϕ is the shear angle, λ is average friction angle at tool chip interface, and θ is the angle between resultant

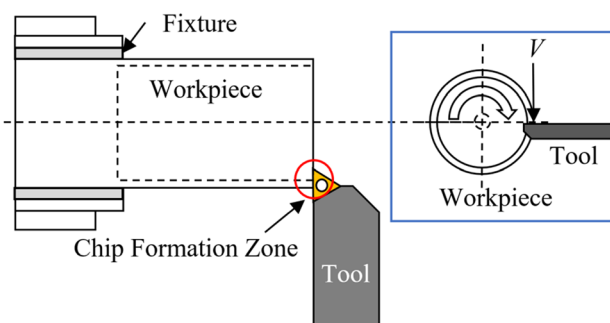


Fig. 1 Schematic drawing of orthogonal cutting in turning a tubular workpiece

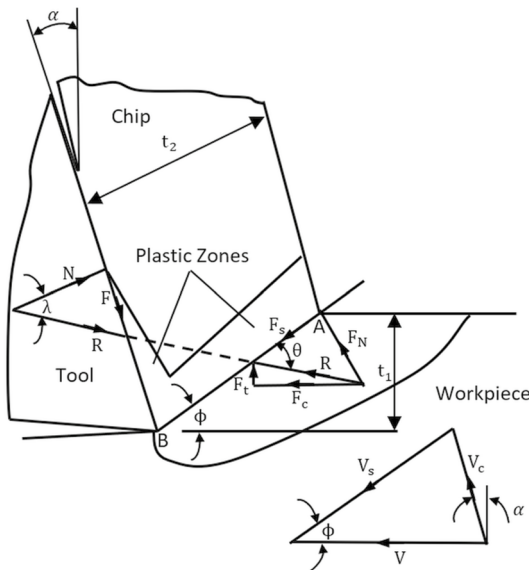


Fig. 2 Chip formation in orthogonal cutting configuration [22]

cutting force R and primary shear zone AB . $t_1 t_2$ are the depth of cut (undeformed chip thickness) and the chip thickness, respectively. V , V_s , V_c are cutting velocity, shear velocity, and chip velocity, respectively. F_c , F_t , R are cutting force, thrust force, and resultant force, respectively. w is the cutting width that is not shown.

Fig. 3 Algorithm of analytical temperature model based on Johnson–Cook model and mechanics of the orthogonal cutting process

With J–C model and cutting mechanics model, the machining temperatures are predicted as illustrated in Fig. 3, where the inputs are J–C constants, experimental cutting force and chip thickness, and cutting condition parameters of cutting velocity, rake angle, the width of cut, and depth of cut. The average temperatures at PSZ and SSZ are outputs. The following assumptions are enforced: (1) steady state and plane strain condition, (2) constant material flow rate at chip formation zone, (3) plane strain condition.

The shear angle is calculated explicitly from the chip compression ratio with the assumption of the constant materials flow rate ($t_1 V = t_2 V_c$) as

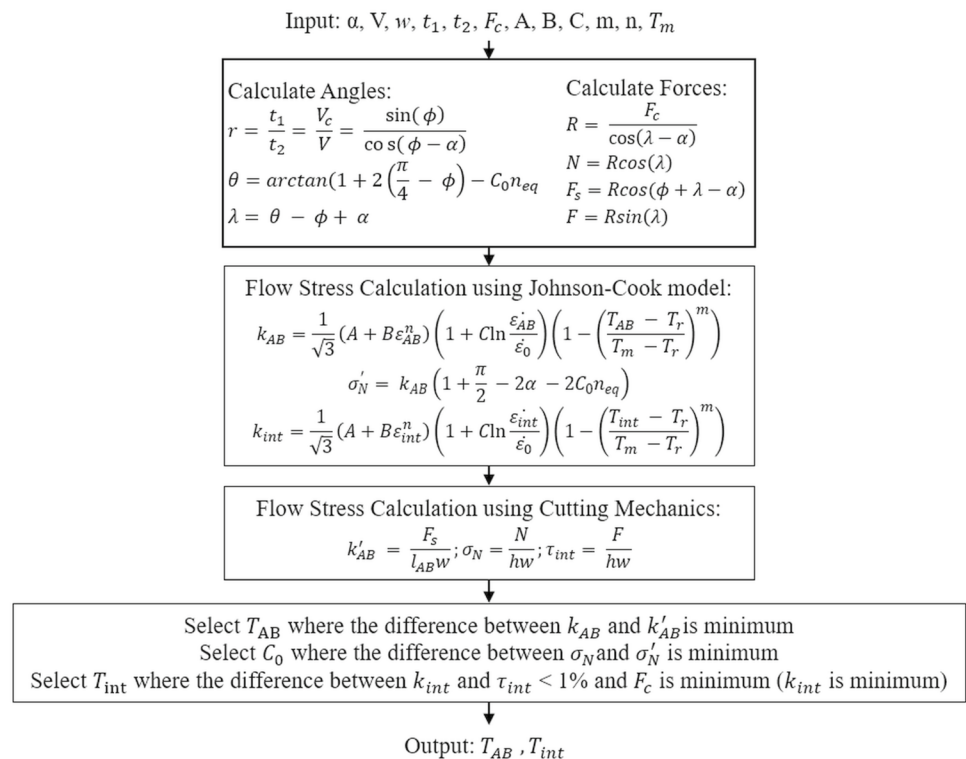
$$r = \frac{t_1}{t_2} = \frac{V_c}{V} = \frac{\sin(\phi)}{\cos(\phi - \alpha)} \quad (2)$$

The other angles in the chip formation zone are calculated as

$$\theta = \arctan\left(1 + 2\left(\frac{\pi}{4} - \phi\right) - C_0 n_{eq}\right) \quad (3)$$

$$\lambda = \theta - \phi + \alpha \quad (4)$$

The shear flow stress at PSZ calculated using J–C model with von Mises yield criterion and cutting mechanics is expressed as



$$\begin{aligned} k'_{AB} &= \frac{\sigma_{AB}}{\sqrt{3}} \\ &= \frac{1}{\sqrt{3}}(A + B\varepsilon_{AB}^n) \left(1 + C \ln \frac{\dot{\varepsilon}_{AB}}{\dot{\varepsilon}_0}\right) \left(1 - \left(\frac{T_{AB} - T_r}{T_m - T_r}\right)^m\right) \end{aligned} \quad (5)$$

$$k_{AB} = \frac{F_s}{l_{AB}w} \quad (6)$$

where the strain and strain rate at PSZ are calculated as

$$\varepsilon_{AB} = \frac{\gamma_{AB}}{\sqrt{3}} = \frac{\cos\alpha}{2\sqrt{3}\sin\phi\cos(\phi - \alpha)} \quad (7)$$

$$\dot{\varepsilon}_{AB} = \frac{\dot{\gamma}_{AB}}{\sqrt{3}} = C_0 \frac{V_s}{\sqrt{3}l_{AB}} \quad (8)$$

The shear flow stress at SSZ calculated using J–C model with von Mises yield criterion and cutting mechanics is expressed as

$$\begin{aligned} k_{int} &= \frac{\sigma_{int}}{\sqrt{3}} \\ &= \frac{1}{\sqrt{3}}(A + B\varepsilon_{int}^n) \left(1 + C \ln \frac{\dot{\varepsilon}_{int}}{\dot{\varepsilon}_0}\right) \left(1 - \left(\frac{T_{int} - T_r}{T_m - T_r}\right)^m\right) \end{aligned} \quad (9)$$

$$\tau_{int} = \frac{F}{hw} \quad (10)$$

where the strain and strain rate at SSZ are calculated as

$$\varepsilon_{int} = \frac{\gamma_{int}}{\sqrt{3}} = \frac{1}{\sqrt{3}} \left(\frac{\cos(\alpha)}{\sin(\phi)\cos(\phi - \alpha)} + \frac{h}{2\delta t_2} \right) \quad (11)$$

$$\dot{\varepsilon}_{int} = \frac{\dot{\gamma}_{int}}{\sqrt{3}} = \frac{1}{\sqrt{3}} \frac{V_c}{\delta t_2} \quad (12)$$

The length of the PSZ and tool–chip interface (SSZ) is calculated as

$$l_{AB} = \frac{t_1}{\sin\phi} \quad (13)$$

$$h = \frac{t_1 \sin\theta}{\cos\lambda \sin\phi} \left(1 + \frac{C_0 n_{eq}}{3 \left(1 + 2 \left(\frac{\pi}{4} - \phi\right) - C_0 n_{eq}\right)}\right) \quad (14)$$

where the strain hardening constants (n_{eq}) can be estimated as

$$n_{eq} \approx \frac{nB\varepsilon_{AB}^n}{(A + B\varepsilon_{AB}^n)} \quad (15)$$

The forces can be calculated using the mechanics of orthogonal cutting as

$$F_c = R\cos(\lambda - \alpha) \quad (16)$$

$$F_t = R\sin(\lambda - \alpha) \quad (17)$$

$$F = R\sin\lambda \quad (18)$$

$$F_s = R\cos(\phi + \lambda - \alpha) \quad (19)$$

The presented model has promising short computational time because of its less mathematical complexity, which allows the in situ temperature prediction and optimization of machining temperature condition through process parameter planning.

Results and discussion

In this work, the machining temperatures in orthogonal cutting of SPD-processed UFG Ti were predicted using the presented temperature model under various cutting conditions. The J–C constants, cutting process parameters, and experimental forces and chip thickness were inputs. The shear angle was solved explicitly from the chip compression ratio with the assumption of constant material flow rate at the chip formation zone. The material properties including thermal conductivity and specific heat were not needed in the temperature model with the inputs of experimental force and chip thickness.

The J–C constants of the UFG Ti were adopted from the previous work as given in Table 1, which were inversely determined based on machining force prediction using the modified chip formation model. An iterative gradient searching method based on Kalman filter algorithm was employed to improve the computational efficiency [24].

The cutting conditions and experimental forces were obtained from the orthogonal cutting experiment, in which a piezoelectric dynamometer was used to measure the machining forces. The experimental chip thickness under each cutting condition was measured in triplicates using a micrometer in this work. The documented temperatures at two shear zones were adopted from the previous work [2] and validated

Table 1 J–C constants of SPD-processed UFG Ti ($T_0 = 25^\circ\text{C}$; $T_m = 1660^\circ\text{C}$; $\dot{\varepsilon}_0 = 1$) [24]

A (MPa)	B (MPa)	n	C	m
451.89	350.22	0.101	0.010	1.484

Table 2 Cutting conditions for orthogonal machining [2]. Superscript R denotes documented value

Test	V (m/min)	w (mm)	t_1 (mm)	F_c (N)	F_t (N)	t_2 (mm)	T_{AB}^R (°C)	T_{int}^R (°C)
1	60	1	0.2	333.83	206.32	0.439	210.73	791.80
2	75	1	0.2	338.14	204.81	0.439	213.92	779.13
3	90	1	0.3	480.38	231.44	0.601	211.84	940.18
4	60	0.5	0.3	302.13	117.52	0.629	210.57	875.04
5	90	0.5	0.4	351.50	118.66	0.767	210.80	1017.30
6	120	0.5	0.4	350.35	124.24	0.767	214.64	1001.90

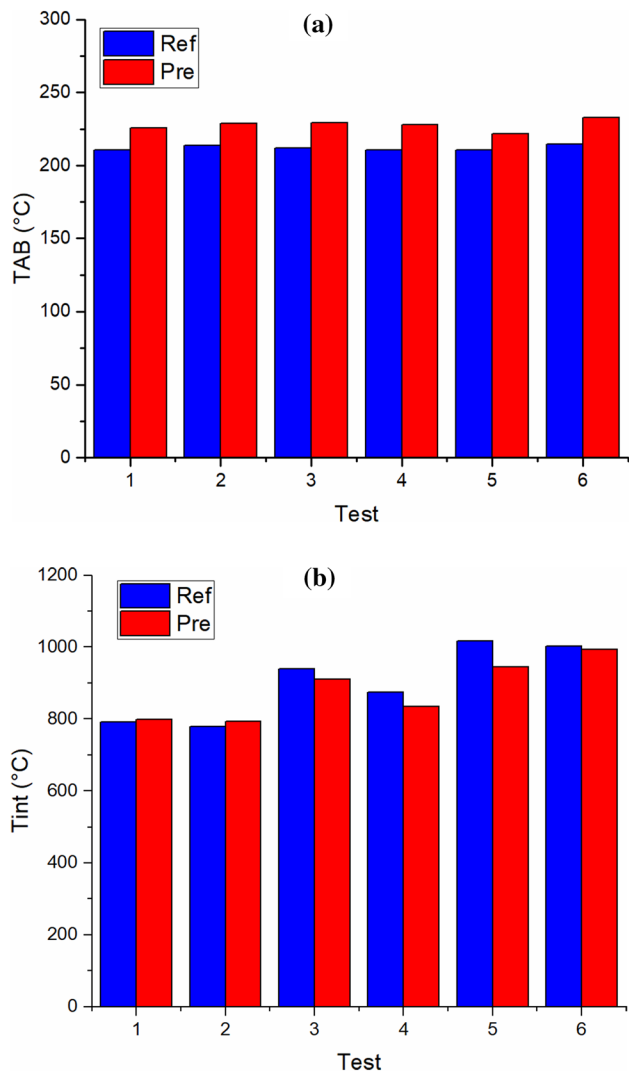


Fig. 4 Validation of predicted temperatures (pre) against reference values (ref) under various cutting conditions. **a** The comparison of temperatures at PSZ and **b** the comparison of temperatures at SSZ

with forces comparison because temperatures were used as intermediate variables in calculating machining forces. The cutting conditions, experimental force, chip thickness, and documented temperatures are given in Table 2.

The predicted temperatures at PSZ and SSZ were validated with documented values in multiple cutting tests

as illustrated in Fig. 4. Close agreements were observed between predicted temperature and documented values. The predicted temperatures at PSZ (T_{AB}) were larger than the documented temperatures because the documented temperatures were predicted by the modified chip formation model with the assumption of the perfectly sharp cutting tool, which resulted in the underestimated machining forces and temperatures. This assumption was not used in the presented model. The predicted temperatures at SSZ (T_{int}) agreed well with documented values. The minor deviations of predicted temperatures might be caused by the deviations of input experimental forces, chip thickness, and adopted J–C constants (Table 3).

The computational time for the temperature prediction using the presented model and the modified chip formation model in the previous work was recorded and compared as given in Table 4. The calculations were carried out using MATLAB program on a personal computer running at 2.8 GHz. The increments of strain rate constants (δ , C_0) were set as 0.05 and 0.1, respectively. In the previous work, the average time for each temperature prediction using the modified chip formation model was 8883 s with an increment of shear angle (ϕ as 0.1°). In this work, the shear angle was solved explicitly from chip compression ratio. The average time for each temperature prediction using the presented model was 0.484 s. Significant improvement on computational time was observed with the presented model because of direct input of forces and chip thickness that allowed the intermediate variables to be calculated explicitly. The promising short computational time allows the process parameter planning through inverse analysis [29, 30]. The model algorithms were compared in terms of input variables, assumptions, and experimental and mathematical complexity as shown in Table 5. The presented model was favored with less experimental and mathematical complexity. Both models have accepted prediction accuracy as illustrated in Fig. 4.

In addition, the predicted temperatures in machining UFG Ti were compared to the temperatures in machining Ti–6Al–4V under the same cutting conditions. Machining temperatures of Ti–6Al–4V were predicted using the modified chip formation model, in which the J–C constants and material properties are needed. The J–C constants

Table 3 Predicted temperatures and related variables

Test	T_{AB} (°C)	T_{int} (°C)	k_{AB} (MPa)	k'_{AB} (MPa)	τ_{int} (MPa)	k_{int} (MPa)	ϕ (°)
1	225.63	797.78	477.91	478.93	366.97	366.97	24.49
2	228.74	794.18	478.38	479.39	367.33	367.33	24.49
3	229.07	910.11	476.55	477.56	326.51	326.51	26.54
4	227.92	835.39	475.35	476.37	346.14	346.14	25.51
5	221.71	944.13	476.16	477.17	304.90	304.89	27.56
6	232.99	993.83	475.55	476.56	304.51	304.51	27.56

Table 4 Quantitative comparison of the computational time in the temperature prediction of UFG Ti

Test	Computational time with modified chip formation model (s) [2]	Computational time with presented model (s)
1	9149	0.494
2	9086	0.492
3	9082	0.466
4	8706	0.483
5	8660	0.486
6	8614	0.482

and materials properties of Ti–6Al–4V were adopted from the literature as given in Table A1 and Table A2, respectively, in Appendix [31, 32]. The temperatures in machining Ti–6Al–4V were higher than the temperatures in machining UFG Ti as shown in Fig. 5. The elevated temperatures in the machining process reduce the tool life and increase material diffusion. This trend agrees with the trend of force comparisons reported in the previous work [2]. The positive correlation between machining force and temperature has also been reported in the literature [20, 21].

The presented model could be further developed for oblique cutting configuration to future improve its usefulness in real applications. The preliminary work has been reported based on the geometrical relationship between orthogonal cutting configuration and oblique cutting configuration in the modified chip formation model [33].

Conclusion

In this work, the machining temperatures of UFG Ti in an integrated manufacturing process combining SPD process and machining process were predicted using an analytical model that was developed based on materials constitutive relation and mechanics of the cutting process. Machining temperatures were predicted under various process conditions in orthogonal cutting tests. Closed agreements were observed between predicted temperatures and documented values. For the machinability in temperature, the machining temperatures of UFG Ti were significantly lower than that of Ti–6Al–4V under the same cutting conditions. Moreover, the average computational time of the presented model was 0.484 s. For comparison, the average computational time with the modified chip formation model in the previous work was 8883 s.

The contributions of these works are (1) to extend the applicability of the original temperature model based on material constitutive relation and mechanics of the cutting process to a broader class of materials; (2) to investigate the machinability in machining temperature in the manufacturing process integrating the SPD process and machining with significantly improved computational efficiency, which allows the *in situ* temperature prediction and optimization of the machining process with process parameters planning; 3) to promote the use of UFG Ti in engineering and biomedical applications with the comparison of machining temperatures to widely used Ti–6Al–4V.

Table 5 Qualitative comparison of the model algorithm in the temperature prediction of UFG Ti

Model	Input variables	Assumptions	Experimental complexity	Mathematical complexity
Modified chip formation model	Cutting parameters; J–C constants; Materials properties; heat partition ratios at PSZ and SSZ	Perfect sharp cutting tool; steady state, plane strain condition	Extensive material property tests	Calculation of temperature, force, and chip thickness, materials flow stress and strain, geometry, and model parameters
Presented model	Cutting parameters; J–C constants; cutting force; chip thickness	Constants materials flow rate at chip formation zone; steady state, plane strain condition	Easily measurable cutting force and chip thickness	Calculations of temperature, materials flow stress, geometry, and model parameters

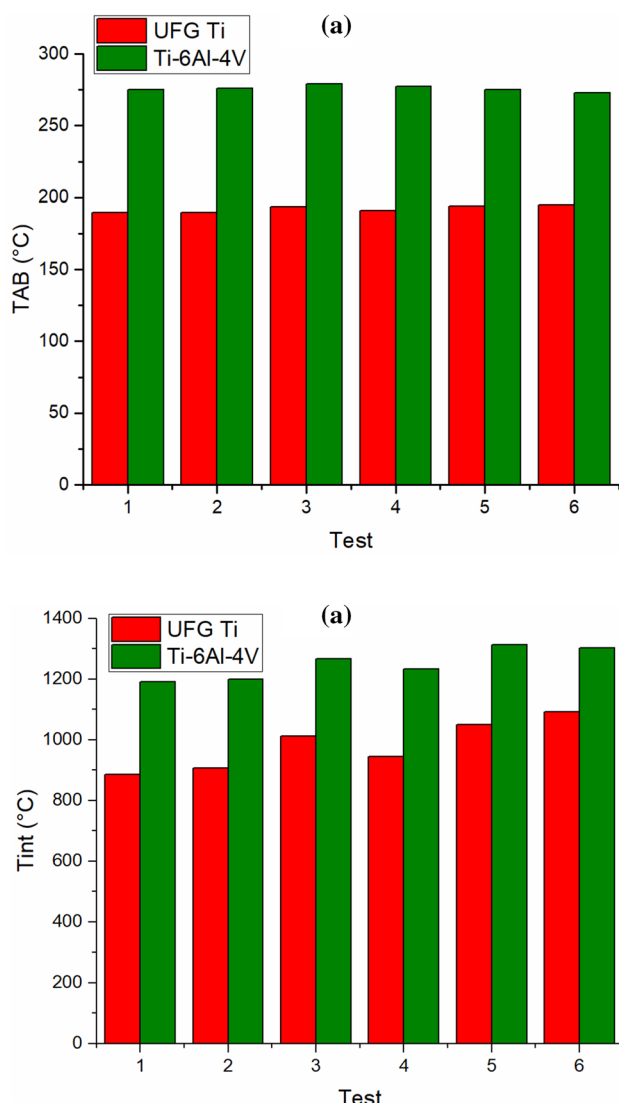


Fig. 5 Comparison between machining temperatures of UFG Ti and machining temperatures of Ti-6Al-4V under various cutting conditions. **a** The comparison of machining temperature at PSZ and **b** the comparison of machining temperatures at SSZ

Compliance with ethical standards

Conflict of interest The authors declare that they have no conflict of interest.

Human and animal rights This article does not contain any studies with human or animal subject performed by any of the authors.

Appendix

See Tables 6 and 7.

Table 6 J–C constants of Ti–6Al–4V ($T_0 = 25$ °C; $\dot{\varepsilon}_0 = 1$) [31]

A (MPa)	B (MPa)	n	C	m
997.9	653.1	0.45	0.0198	0.7

Table 7 Materials properties of Ti–6Al–4V [32]

ρ (kg/m ³)	T_m (°C)	C_p (J/kg °C)	K (w/m °C)
4420	1668	560	9.2

References

- Elias CN, Meyers MA, Valiev RZ, Monteiro SN (2013) Ultra fine grained titanium for biomedical applications: an overview of performance. *J Mater Res Technol* 2(4):340–350. <https://doi.org/10.1016/j.jmrt.2013.07.003>
- Ning J, Nguyen V, Liang SY (2018) Analytical modeling of machining forces of ultra-fine-grained titanium. *The Int J Adv Manuf Technol* 101(1–4):627–636. <https://doi.org/10.1007/s00170-018-2889-6>
- Anselme K, Noe B, Hardouin P (1999) Human osteoblast adhesion on titanium alloy, stainless steel, glass and plastic substrates with same surface topography. *J Mater Sci Mater Med* 10(12):815–819. <https://doi.org/10.1023/A:1008992109670>
- Stolyarov VV, Zhu YT, Alexandrov IV, Lowe TC, Valiev RZ (2001) Influence of ECAP routes on the microstructure and properties of pure Ti. *Mater Sci Eng A* 299(1–2):59–67. [https://doi.org/10.1016/S0921-5093\(00\)01411-8](https://doi.org/10.1016/S0921-5093(00)01411-8)
- Stolyarov VV, Zhu YT, Lowe TC, Valiev RZ (2001) Microstructure and properties of pure Ti processed by ECAP and cold extrusion. *Mater Sci Eng A* 303(1–2):82–89. [https://doi.org/10.1016/S0921-5093\(00\)01884-0](https://doi.org/10.1016/S0921-5093(00)01884-0)
- Stolyarov VV, Zhu YT, Alexandrov IV, Lowe TC, Valiev RZ (2003) Grain refinement and properties of pure Ti processed by warm ECAP and cold rolling. *Mater Sci Eng A* 343(1–2):43–50. [https://doi.org/10.1016/S0921-5093\(02\)00366-0](https://doi.org/10.1016/S0921-5093(02)00366-0)
- Horita Z, Fujinami T, Langdon TG (2001) The potential for scaling ECAP: effect of sample size on grain refinement and mechanical properties. *Mater Sci Eng A* 318:34–41. [https://doi.org/10.1016/S0921-5093\(01\)01339-9](https://doi.org/10.1016/S0921-5093(01)01339-9)
- Longbottom JM, Lanham JD (2005) Cutting temperature measurement while machining—a review. *Aircr Eng Aerosp Technol* 77(2):122–130. <https://doi.org/10.1108/00022660510585956>
- Komanduri R, Hou ZB (2001) A review of the experimental techniques for the measurement of heat and temperatures generated in some manufacturing processes and tribology. *Tribol Int* 34(10):653–682. [https://doi.org/10.1016/S0301-679X\(01\)00068-8](https://doi.org/10.1016/S0301-679X(01)00068-8)
- Umbrello D, M'saoubi R, Outeiro JC (2007) The influence of Johnson–Cook material constants on finite element simulation of machining of AISI 316L steel. *Int J Mach Tools Manuf* 47(3–4):462–470. <https://doi.org/10.1016/j.ijmachtools.2006.06.006>
- Özel T, Ulutan D (2012) Prediction of machining induced residual stresses in turning of titanium and nickel based alloys with experiments and finite element simulations. *CIRP Ann-Manuf Technol* 61(1):547–550. <https://doi.org/10.1016/j.cirp.2012.03.100>
- Gonzalo O, Jauregi H, Uriarte LG, de Lacalle LL (2009) Prediction of specific force coefficients from a FEM cutting model. *Int J Adv Manuf Technol* 43(3–4):348. <https://doi.org/10.1007/s00170-008-1717-9>

13. Danish M, Ginta TL, Habib K, Carou D, Rani AMA, Saha BB (2017) Thermal analysis during turning of AZ31 magnesium alloy under dry and cryogenic conditions. *Int J Adv Manuf Technol* 91(5–8):2855–2868. <https://doi.org/10.1007/s00170-016-9893-5>
14. Guo YB, Yen DW (2004) A FEM study on mechanisms of discontinuous chip formation in hard machining. *J Mater Process Technol* 155:1350–1356. <https://doi.org/10.1016/j.jmatprotec.2004.04.210>
15. Feng Y, Lu YT, Lin YF et al (2018) Inverse analysis of the cutting force in laser-assisted milling on Inconel 718. *Int J Adv Manuf Technol* 96(1–4):905–914. <https://doi.org/10.1007/s00170-018-1670-1>
16. Ning J, Liang SY (2019) Predictive modeling of machining temperatures with force-temperature correlation using cutting mechanics and constitutive relation. *Mater* 12(2):284. <https://doi.org/10.3390/ma12020284>
17. Ning J, Liang S (2018) Prediction of temperature distribution in orthogonal machining based on the mechanics of the cutting process using a constitutive model. *J Manuf Mater Process* 2(2):37. <https://doi.org/10.3390/jmmp2020037>
18. Ning J, Liang S (2018) Evaluation of an analytical model in the prediction of machining temperature of AISI 1045 steel and AISI 4340 steel. *J Manuf Mater Process* 2(4):74. <https://doi.org/10.3390/jmmp2040074>
19. Ning J, Liang SY (2019) A comparative study of analytical thermal models to predict the orthogonal cutting temperature of AISI 1045 steel. *Int J Adv Manuf Technol* 102(9–12):3109–3119. <https://doi.org/10.1007/s00170-019-03415-9>
20. Shalaby MA, El Hakim MA, Veldhuis SC (2018) A thermal model for hard precision turning. *Int J Adv Manuf Technol* 98:2401–2413. <https://doi.org/10.1007/s00170-018-2389-8>
21. Lalwani DI, Mehta NK, Jain PK (2009) Extension of Oxley's predictive machining theory for Johnson and Cook flow stress model. *J Mater Process Technol* 209(12–13):5305–5312. <https://doi.org/10.1016/j.jmatprotec.2009.03.020>
22. Oxley PLB (1989) The Mechanics of machining: an analytical approach to assessing machinability. Ellis Horwood, London
23. Komanduri R, Hou ZB (2001) Thermal modeling of the metal cutting process—part III: temperature rise distribution due to the combined effects of shear plane heat source and the tool–chip interface frictional heat source. *Int J Mech Sci* 43(1):89–107. [https://doi.org/10.1016/S0020-7403\(99\)00105-8](https://doi.org/10.1016/S0020-7403(99)00105-8)
24. Ning J, Nguyen V, Huang Y, Hartwig KT, Liang SY (2018) Inverse determination of Johnson–Cook model constants of ultra-fine-grained titanium based on chip formation model and iterative gradient search. *Int J Adv Manuf Technol* 99(5–8):1131–1140. <https://doi.org/10.1007/s00170-018-2508-6>
25. Ivester RW, Kennedy M, Davies M, Stevenson R, Thiele J, Furness R, Athavale S (2000) Assessment of machining models: progress report. *Mach Sci Technol* 4(3):511–538. <https://doi.org/10.1080/10940340008945720>
26. Kolsky H (1949) An investigation of the mechanical properties of materials at very high rates of loading. *Proc Phys Soc Sect B* 62(11):676
27. Shrot A, Bäker M (2012) Determination of Johnson–Cook parameters from machining simulations. *Comput Mater Sci* 52(1):298–304. <https://doi.org/10.1016/j.commatsci.2011.07.035>
28. Agnelli M, Ahadi A, Ståhl JE (2014) Identification of plasticity constants from orthogonal cutting and inverse analysis. *Mech Mater* 77:43–51. <https://doi.org/10.1016/j.mechmat.2014.07.005>
29. Ning J, Liang SY (2018) Model-driven determination of Johnson–Cook material constants using temperature and force measurements. *Int J Adv Manuf Technol* 97(1–4):1053–1060. <https://doi.org/10.1007/s00170-018-2022-x>
30. Ning J, Liang SY (2019) Inverse identification of Johnson–Cook material constants based on modified chip formation model and iterative gradient search using temperature and force measurements. *Int J Adv Manuf Technol* 102(9–12):2865–2876. <https://doi.org/10.1007/s00170-019-03286-0>
31. Seo S, Min O, Yang H (2005) Constitutive equation for Ti–6Al–4V at high temperatures measured using the SHPB technique. *Int J Impact Eng* 31(6):735–754. <https://doi.org/10.1016/j.ijimpeng.2004.04.010>
32. Boivineau M, Cagran C, Doytier D, Eyrard V, Nadal MH, Wilthan B, Pottlacher G (2006) Thermophysical properties of solid and liquid Ti–6Al–4V (TA6 V) alloy. *Int J Thermophys* 27(2):507–529. <https://doi.org/10.1007/PL00021868>
33. Pan Z, Lu YT, Lin YF, Hung TP, Hsu FC, Liang SY (2017) Analytical model for force prediction in laser-assisted milling of IN718. *Int J Adv Manuf Technol* 90(9–12):2935–2942. <https://doi.org/10.1007/s00170-016-9629-6>